

# Comprehensive understanding on phosphorus precipitation in heavily phosphorus-doped Czochralski silicon

Cite as: J. Appl. Phys. 134, 155701 (2023); doi: 10.1063/5.0161897

Submitted: 12 June 2023 · Accepted: 30 September 2023 ·

Published Online: 17 October 2023



View Online



Export Citation



CrossMark

Defan Wu,<sup>1</sup> Tong Zhao,<sup>1</sup> Bin Ye,<sup>2</sup> Hao Chen,<sup>1</sup> Xingbo Liang,<sup>2</sup> Shenzhong Li,<sup>1,2</sup> Daxi Tian,<sup>2</sup> Deren Yang,<sup>1</sup> and Xiangyang Ma<sup>1,a)</sup>

## AFFILIATIONS

<sup>1</sup>State Key Laboratory of Silicon and Advanced Semiconductor Materials and School of Materials Science and Engineering, Zhejiang University, Hangzhou 310027, China

<sup>2</sup>QL Electronics Science (Quzhou) Co., Ltd, No. 52, Panlong South Road, Quzhou 324000, China

<sup>a)</sup>Author to whom correspondence should be addressed: [mxyoung@zju.edu.cn](mailto:mxyoung@zju.edu.cn).

## ABSTRACT

Heavily phosphorus-doped Czochralski (HP-CZ) silicon is an important substrate material for manufacturing power electronic devices. The high concentration of phosphorus impurities may be supersaturated during the crystal growth of HP-CZ silicon or device manufacturing. Thus, understanding phosphorus precipitation in HP-CZ silicon is of technological significance. Herein, a panoramic view of phosphorus precipitation in HP-CZ silicon is presented in terms of crystallography, thermodynamics, and kinetics. It is found that the orthorhombic SiP precipitates can form during the crystal growth of HP-CZ silicon and also during the post-anneals of HP-CZ silicon at 450–1050 °C. Along with increasing annealing temperature, the formed SiP precipitates tend to adopt the platelet, polyhedron, and sphere-like shapes. Moreover, the excess point defects, i.e., silicon self-interstitials and vacancies, are found to affect phosphorus precipitation occurring in the low and high temperature regimes in different ways. In light of the kinetics of phosphorus precipitation at different temperatures, it is deduced that phosphorus precipitation follows a growth law in compliant with Ham's theory to a large extent. As an important output of this work, the temperature-dependent phosphorus solubilities in the dislocation-free silicon, which have been hardly acquired previously, are derived on the basis of investigating phosphorus precipitation in a set of HP-CZ silicon wafers with different phosphorus concentrations. Moreover, the derived solvus line for the phosphorus impurities in silicon could be a beneficial supplement to the existing phase diagram of the Si-P binary system in the extremely silicon-rich corner.

21 October 2023 10:19:51

Published under an exclusive license by AIP Publishing. <https://doi.org/10.1063/5.0161897>

## I. INTRODUCTION

Heavily phosphorus-doped Czochralski (HP-CZ) silicon wafers, which are dislocation-free, are widely used as the substrates of epitaxial silicon wafers used for manufacturing power electronic devices. In order to reduce the on-resistance of the devices, nowadays, the HP-CZ silicon wafers are required to possess the resistivities of no more than  $1.5 \text{ m}\Omega \text{ cm}$ . However, there should be a lower limit of resistivity for dislocation-free HP-CZ silicon. Chiou experimentally derived that the dislocations would inevitably form during the growth of HP-CZ silicon ingot as the phosphorus concentration exceeds  $8.2 \times 10^{19} \text{ cm}^{-3}$ , which corresponds to a resistivity of  $0.92 \text{ m}\Omega \text{ cm}$ .<sup>1</sup> Currently, the commercially available HP-CZ silicon

wafers used for the power electronic devices are generally with the resistivities in the range of  $1\text{--}1.5 \text{ m}\Omega \text{ cm}$ , which are corresponding to the phosphorus concentrations ranging from  $\sim 4.6$  to  $7.4 \times 10^{19} \text{ cm}^{-3}$ . The phosphorus impurities with such high concentrations in the HP-CZ silicon wafers may be supersaturated during the thermal cycles of device fabrication. In this case, a fraction of the phosphorus impurities perhaps precipitate out of the silicon matrix; that is, the so-called phosphorus precipitation may occur. Naturally, studying phosphorus precipitation in HP-CZ silicon and its underlying mechanism is of technological significance.

In fact, the investigation on phosphorus precipitation in HP-CZ silicon can date back to 1976 to our knowledge. In that

year, by combining the electrical measurements and transmission electron microscopy (TEM) observation, Ostoja *et al.* supposed that phosphorus precipitation, namely, the formation of silicon phosphide (SiP) precipitates, occurred in HP-CZ silicon doped with a phosphorus concentration of  $7.5 \times 10^{19} \text{ cm}^{-3}$ , subjected to isochronal anneal of 500 h at 550 °C.<sup>2</sup> However, they did not provide solid evidence for the designation of the SiP phase. Moreover, they did not observe phosphorus precipitation in HP-CZ silicon doped with the phosphorus concentration from  $1.7$  to  $5.8 \times 10^{19} \text{ cm}^{-3}$ , subjected to the isochronal anneal of 500 h at temperatures ranging from 400 to 775 °C. For a long time thereafter, there were few reports on phosphorus precipitation in HP-CZ silicon. By 2006, Zeng *et al.* reported that phosphorus precipitation occurred in HP-CZ silicon with a phosphorus concentration of  $4.6 \times 10^{19} \text{ cm}^{-3}$ , subjected to 650 °C anneal for 8 h, following a prior high-temperature anneal at 1230 °C for 15 min.<sup>3</sup> Up to now, whether phosphorus precipitation can be enabled in HP-CZ silicon by the isochronal anneal at temperatures above 650 °C remains unknown. Nevertheless, it should be noted that phosphorus precipitation was found to occur in the thermal-diffused or ion-implanted phosphorus regions, usually with very high concentrations in the order of  $10^{20-21} \text{ cm}^{-3}$ , within a lightly doped silicon substrate when subjected to the anneal at an elevated temperature ranging 900–1050 °C, and thus-formed precipitates were confirmed to be of a monoclinic or orthorhombic SiP phase.<sup>4-6</sup> Generally, the thermal-diffused or ion-implanted phosphorus regions contain numerous dislocations generated by the appreciable misfit stresses arisen from the extremely high concentration of doped phosphorus impurities. Such dislocations can act as the fast-diffusing channels for the phosphorus impurities and provide the heterogeneous nucleation sites, thus facilitating phosphorus precipitation. In this work, the investigated HP-CZ silicon wafers are dislocation-free and their phosphorus concentrations are 1–2 orders of magnitude lower than those in thermal-diffused or ion-implanted phosphorus regions. Then, is it possible for phosphorus precipitation to occur in HP-CZ silicon when subjected to the anneals at the elevated temperatures, especially at 900–1050 °C? Addressing this issue represents the starting point of this work.

It is understandable that the first prerequisite for phosphorus precipitation is that the phosphorus concentration in HP-CZ silicon should exceed the phosphorus solubility in silicon at a given

temperature. At present, there have been widely accepted data of phosphorus solubilities in silicon.<sup>7–10</sup> Generally, the acquisitions of such phosphorus solubilities were based on thermal diffusion and ion implantation processes. As mentioned above, the thermal-diffused or ion-implanted phosphorus regions usually contain numerous dislocations, which can accommodate appreciable amounts of phosphorus impurities besides the substitutional ones in the lattice of silicon. Intuitively, the phosphorus solubilities in the dislocation-free silicon should be much smaller than the existing data. Based on a series of reported phosphorus solubilities, Solmi *et al.* once derived an expression:  $C_{\text{sat}} = 2.45 \times 10^{23} \exp(-0.62 \text{ eV}/kT) \text{ cm}^{-3}$ , where  $C_{\text{sat}}$  represents the phosphorus solubility at a given temperature.<sup>8</sup> According to this expression, the phosphorus solubility at 1050 °C is  $1.07 \times 10^{21} \text{ cm}^{-3}$ , far exceeding the reported upper limit of phosphorus concentration,  $8.2 \times 10^{19} \text{ cm}^{-3}$ , in the dislocation-free HP-CZ silicon.<sup>1</sup> Moreover, as will be reported below, phosphorus precipitation can even occur at 1050 °C in the dislocation-free HP-CZ silicon with a phosphorus concentration of  $7.35 \times 10^{19} \text{ cm}^{-3}$ . Therefore, the above-mentioned two facts definitely indicate that the existing phosphorus solubility data are, indeed, not appropriate for the dislocation-free silicon. Unfortunately, this issue has not been addressed until now.

In this work, phosphorus precipitation behaviors in HP-CZ silicon subjected to the appropriate length of anneals at 450–1050 °C have been systematically investigated. The resulting precipitates have been substantially characterized in terms of crystallography and morphology. Moreover, the effects of excess point defects including vacancies and silicon interstitials on phosphorus precipitation have been revealed. The thermodynamic analyses have been rigorously made to understand the nucleation for phosphorus precipitation. From the kinetics point of view, the effect of oxygen precipitation on phosphorus precipitation and the growth law for phosphorus precipitation have been tentatively revealed. Of technological significance, we have attempted to derive the dependence of phosphorus solubility on temperature for the dislocation-free silicon for the first time based on investigating phosphorus precipitation behaviors in a set of HP-CZ silicon wafers with different phosphorus concentrations. In brief, the present work offers a panoramic view of phosphorus precipitation in HP-CZ silicon.

21 October 2023 10:19:51

## II. EXPERIMENTAL

Seven 300 mm-diameter, ⟨100⟩ oriented, double-side mirror-polished HP-CZ silicon wafers, numbered HP1–7, were used. The resistivities of the seven HP-CZ silicon wafers range from 1.01 to 3.91 mΩ cm, which were measured by a four-point probe. The phosphorus concentrations in the seven HP-CZ silicon wafers were measured by a Cameca 4f secondary ion mass spectrometer (SIMS). Detailed information on the seven HP-CZ silicon wafers is listed in Table I. For different annealing schemes, a few of  $15 \times 15 \text{ mm}^2$  sized specimens were cleaved from each of the seven HP-CZ silicon wafers. All the specimens were first subjected to a so-called homogenization anneal at 1250 °C for 30 min in an argon (Ar) ambience to substantially eliminate the thermal history. For the convenience of description, this homogenization anneal will not be mentioned anymore hereafter. Moreover, it should be mentioned that HP1 wafer was used for all the experiments and HP2–7 wafers were only used for the experiment in Sec. III E.

**TABLE I.** Resistivities and phosphorus concentrations of the HP-CZ silicon wafers used.

Wafer no.	Resistivity (mΩ cm)	Phosphorus concentration (cm <sup>-3</sup> )	(at. %)
HP1	1.01	$7.35 \times 10^{19}$	0.147
HP2	1.17	$6.20 \times 10^{19}$	0.124
HP3	1.30	$5.64 \times 10^{19}$	0.113
HP4	1.75	$3.79 \times 10^{19}$	0.0758
HP5	2.16	$3.06 \times 10^{19}$	0.0612
HP6	3.30	$2.13 \times 10^{19}$	0.0426
HP7	3.91	$1.55 \times 10^{19}$	0.0310

In order to study the effects of point defects on the possible phosphorus precipitation in HP-CZ silicon, some specimens received a prior rapid thermal anneal (RTA) at 1250 °C for 60 s in an Ar ambience for introducing vacancies or prior thermal oxidation at 1100 °C for 4 h in a dry oxygen ambience for injecting interstitial silicon ( $\text{Si}_i$ ) atoms into the bulk of specimens.<sup>11–13</sup> For RTA as mentioned above, the heating rate was 50 °C/s and the average cooling rate from 1250 to 800 °C was 40 °C/s. For different experimental purposes, the annealing schemes for the specimens were implemented at different temperatures in the range of 450–1050 °C for a time ranging 4–512 h. Herein, the shorter times were generally corresponding to the higher temperatures. The electron concentrations in each specimen before and after one of the aforementioned annealing schemes were measured by a Lakeshore 7604 Hall effect measurement system with the van der Pauw configuration.<sup>14</sup> Most of the annealed specimens were preferentially etched in a Yang1 etchant [HF (49%):  $\text{CrO}_3$  (0.5 M) = 1:1] at room temperature for 10 min,<sup>15</sup> followed by observation under an Olympus MX50 optical microscope (OM) equipped with a CCD camera. For the morphological and structural characterizations for phosphorus precipitation in HP-CZ silicon, the specimens subjected to the 450 °C/512 h, 550 °C/256 h, 650–850 °C/32 h, 950 °C/16 h, and 1000–1050 °C/4 h anneals, respectively, were first thinned to be electronically transparent by successive mechanical thinning and ion-milling. Subsequently, they were characterized with a FEI Tecnai G2 F20 S-Twin electron microscope operated at 200 kV, equipped with an energy dispersive spectrometry (EDS) system.

### III. RESULTS AND DISCUSSION

#### A. Electrical deactivation of phosphorus impurities

Figure 1 shows the decreased electron concentration in the HP-CZ silicon specimen subjected to the annealing scheme of 450 °C/512 h, 550 °C/256 h, 650–850 °C/32 h, 950 °C/16 h, or 1000–1050 °C/4 h. The decrease in the electron concentration due to a given anneal as mentioned above represents that a certain number of substitutional phosphorus impurities, which are electrically active as the donors in silicon, depart from the lattice sites. Such a part of phosphorus impurities ultimately precipitates out of the silicon lattice during each of the aforementioned anneals, as will be mentioned later. Evidently, the lower the temperature, the smaller the phosphorus diffusivity is and the more difficult the substitutional phosphorus impurities depart from the lattice sites. Therefore, considerably long annealing times such as 512 and 256 h were used for the anneals at 450 and 550 °C, respectively, to enable the appreciable electrical deactivation of phosphorus impurities, while quite a short annealing time of 4 h at 1000 or 1050 °C was enough for the detectable electrical deactivation of phosphorus impurities. By the way, it is mentioned that no electrical deactivation of phosphorus impurities was found in HP-CZ silicon when annealed at 1100 °C and above. In short, sufficiently long time anneal at a temperature in the range of 450–1050 °C can result in a decrease in the electron concentration in HP-CZ silicon, which is actually due to phosphorus precipitation, as will be verified below.

#### B. Phosphorus precipitation at 450–1050 °C

The OM images for the preferential etching pits in the annealed specimens that gave the results of Fig. 1 are shown in

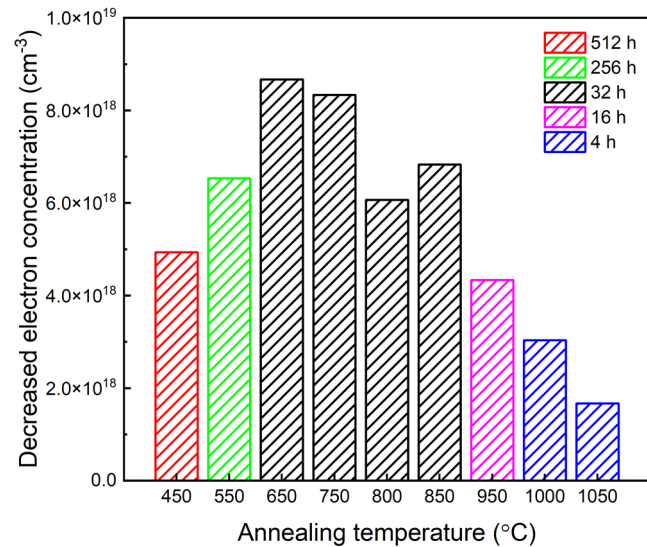


**FIG. 1.** Decreased electron concentration in the HP-CZ silicon specimen subjected to 450 °C/512 h, 550 °C/256 h, 650–850 °C/32 h, 950 °C/16 h, or 1000–1050 °C/4 h anneal.

Figs. 2(a1)–2(i1). As can be seen, a number of etching pits emerge in each annealed specimen, indicating that certain defects are generated by each isothermal anneal as indicated in Fig. 1. Generally, the lower the annealing temperature, the higher the density of the etching pits and, therefore, the generated defects. In the representative TEM image for each annealed specimen, as shown in Figs. 2(a2)–2(i2), a defect in the form of a precipitate can be found. Such a defect is indeed a SiP precipitate, as will be proved by a series of TEM characterizations. In principle, silicon oxide ( $\text{SiO}_x$ ,  $x < 2$ ) precipitates may also form in the annealed specimens as mentioned above. However, the  $\text{SiO}_x$  precipitates were hardly found during our TEM observations. Actually, as will be shown in Fig. 9 later on, the isothermal anneals as indicated in Fig. 1 are believed not to substantially enable oxygen precipitation in HP-CZ silicon. Therefore, it is reasonable to believe that the etching pits manifested in the OM images are primarily related to the SiP precipitates formed in the annealed specimens. So far, it is understandable that the decrease in the electron concentration in each annealed HP-CZ silicon specimen, as shown in Fig. 1, is essentially resulted from phosphorous precipitation.

As can be derived from Figs. 2(a1)–2(f1), considerably dense SiP precipitates are generated by the isothermal anneal of 450 °C/512 h, 550 °C/256 h, or 650–850 °C/32 h. This is attributed to the high supersaturation and small diffusivity of phosphorus impurities at a low temperature in the range of 450–850 °C. However, as shown in Figs. 2(g1)–2(i1), the SiP precipitate density is remarkably decreased as the isothermal anneal is performed at an elevated temperature in the range of 950–1050 °C, which features the low supersaturation and large diffusivity of phosphorus impurities. Moreover, it should be noted that, with the increase in the annealing temperature, the TEM morphology of the SiP

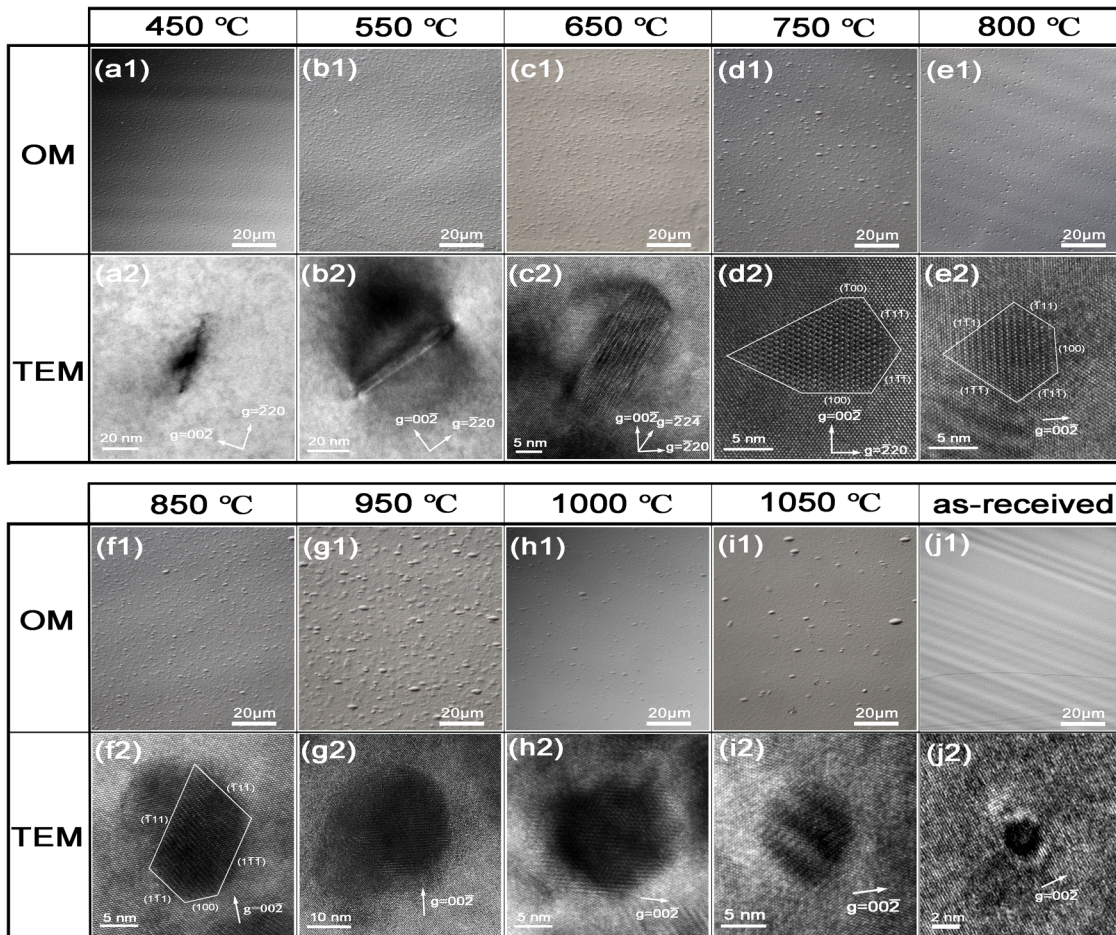


**FIG. 2.** OM images for the preferential etching pits and the representative TEM images for the defects in the annealed specimens that gave the results of Fig. 1 and in the as-received specimen.

21 October 2023 10:19:51

precipitate changes from platelet [Figs. 2(a2)–2(c2)], polyhedron [Figs. 2(d2)–2(f2)] to sphere-like shape [Figs. 2(g2)–2(i2)]. The underlying mechanism for the temperature-dependent morphology of the SiP precipitate will be elucidated later. For the as-received specimen (i.e., without any post-anneal), although few etching pits are delineated [Fig. 2(j1)], the TEM observation in combination with the EDS analysis reveal a sphere-like SiP precipitate with a diameter of  $\sim 3$  nm [Fig. 2(j2)].

### C. Crystal structures of SiP precipitates

Figure 3 shows a series of TEM characterization results for a precipitate generated in the HP-CZ silicon specimen subjected to  $650\text{ }^{\circ}\text{C}/32\text{ h}$  anneal. As shown in Fig. 3(a), the precipitate embedded into the silicon matrix is well crystalline in nature. Moreover, the precipitate and the silicon matrix are semi-coherent in  $[2\bar{2}4]$  orientation while coherent in other orientations of the silicon matrix. Besides, the precipitate features distorted lattice fringes due

to the compressive stress imposed by the silicon matrix. The EDS areal mapping results, as shown in Figs. 3(b) and 3(c), indicate that the precipitate is rich in phosphorus elements and is deficient in silicon elements compared with the silicon matrix. Moreover, the distribution of the oxygen element in the precipitate is almost the same as that in the silicon matrix, as can be seen from Fig. 3(d). Accordingly, it can be believed that the precipitate is of silicon phosphide rather than silicon oxide. In principle, the silicon phosphide could be formulated as  $\text{SiP}$  or  $\text{SiP}_2$ . Considering that the phosphorus concentration in HP-CZ silicon is far from enough for the formation of the  $\text{SiP}_2$  phase according to the  $\text{Si-P}$  binary phase diagram,<sup>16</sup> it is derived that the silicon phosphide precipitate formed in HP-CZ silicon is of the  $\text{SiP}$  phase. Due to the small size of the aforementioned SiP precipitate, the systematic tilting during the HRTEM observation on the SiP precipitate could only be performed along the two zone axes of  $[110]$  and  $[130]$  of the silicon matrix, respectively. Figures 3(e) and 3(f) illustrate the two diffraction patterns that are derived from the HRTEM images of the

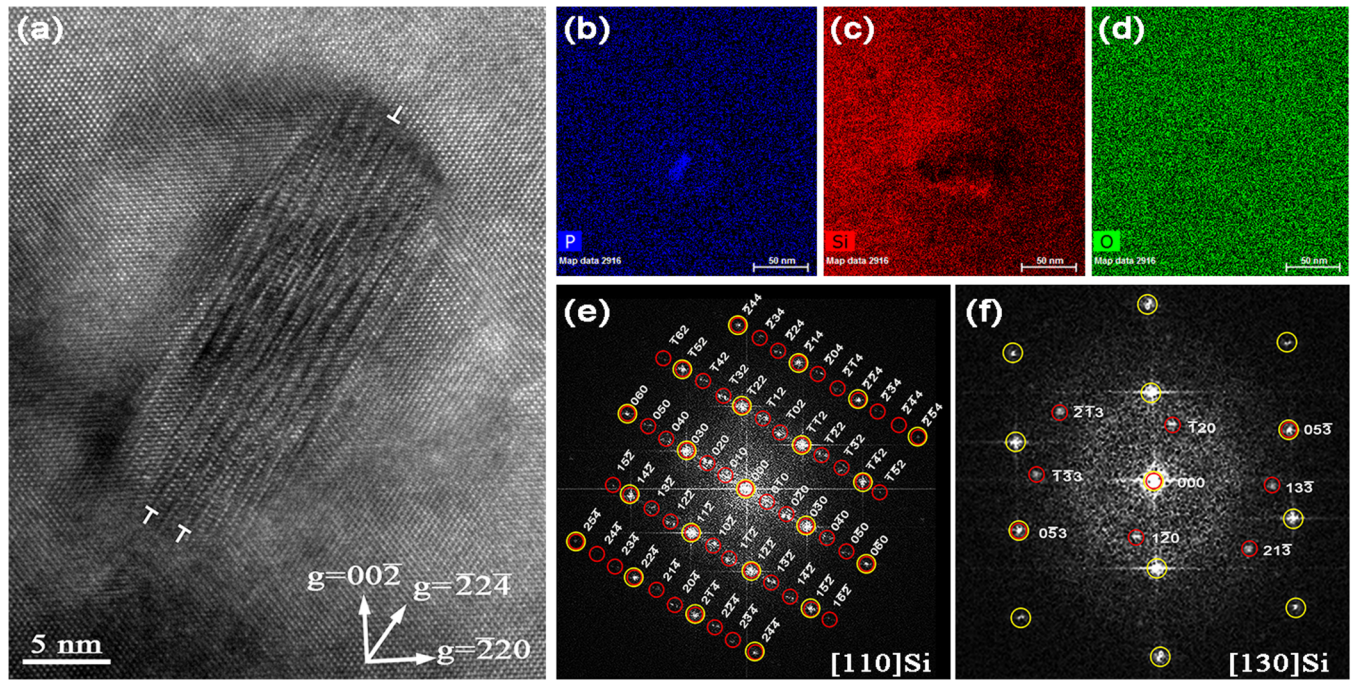


**FIG. 3.** (a) HRTEM image of a precipitate generated in the HP-CZ silicon specimen subjected to 650 °C/32 h anneal, (b)–(d) EDS areal mapping of P, Si, and O elements in the precipitate and silicon matrix, and (e) and (f) FFT diffraction patterns derived from the two HRTEM images of the SiP precipitate, taken along [110] and [130] orientations of the silicon matrix, respectively.

21 October 2023 10:19:51

precipitate, taken along [110] and [130] zone axes of the silicon matrix, respectively, by means of fast Fourier transform (FFT). As can be seen, each diffraction pattern is manifested with a set of spots pertaining to the silicon matrix (marked by the yellow circles) and with another set of spots to the SiP precipitate (marked by the red circles). Through indexing the primary diffraction spots

belonging to the SiP precipitate, as shown in Figs. 3(e) and 3(f), the crystal structure of the SiP precipitate should be assigned to be orthorhombic. Actually, the orthorhombic SiP precipitates were reported to exist in the heavily phosphorus-doped regions within the silicon wafers subjected to the thermal diffusion or the ion implantation of phosphorus impurities.<sup>4,5,17,18</sup> The inter-planar distances of the indexed planes shown in Figs. 3(e) and 3(f) are listed in Table II. On this basis, the lattice parameters for the orthorhombic SiP precipitate, refined by the least squares method, can be ultimately deduced as  $a = 6.47 \text{ \AA}$ ,  $b = 9.35 \text{ \AA}$ , and  $c = 7.56 \text{ \AA}$ . Furthermore, based on the rule of systematic absences, it is found that there are no systematic absences of  $(hkl)$  spots in Figs. 3(e) and 3(f), indicating that the SiP precipitate has a primitive crystal lattice. However, there are 30 space groups of primitive crystal lattice, and several of them such as P222, Pmm2, and Pmmm cannot be distinguished through the reflection conditions.<sup>19</sup> Generally, the orientation relationship between the silicon matrix and the SiP precipitate can be described as  $[110]\text{Si} // [201]\text{SiP}$  and  $[130]\text{Si} // [635]\text{SiP}$ .

Figure 4 shows a series of TEM characterization results for a precipitate generated in the HP-CZ silicon specimen subjected to 950 °C/16 h anneal. As shown in Fig. 4(a), the precipitate embedded into the silicon matrix is also well crystalline in nature. Moreover, the precipitate and the silicon matrix are nearly coherent, thus resulting in little distorted lattice of the precipitate. Likewise, the EDS areal mapping results of phosphorus, silicon,

**TABLE II.** Interplanar distances of the indexed planes of the SiP precipitate shown in Figs. 3(e) and 3(f).

hkl	do (Å)	hkl	do (Å)
010	9.35	053	1.50
020	4.67	204	1.62
120	3.80	214	1.59
102	3.23	152	1.57
030	3.11	060	1.55
112	3.05	224	1.52
122	2.64	234	1.45
040	2.36	162	1.38
132	2.21	244	1.33
213	1.95	254	1.24
133	1.90	172	1.23
142	1.87	264	1.13
050	1.82	...	...

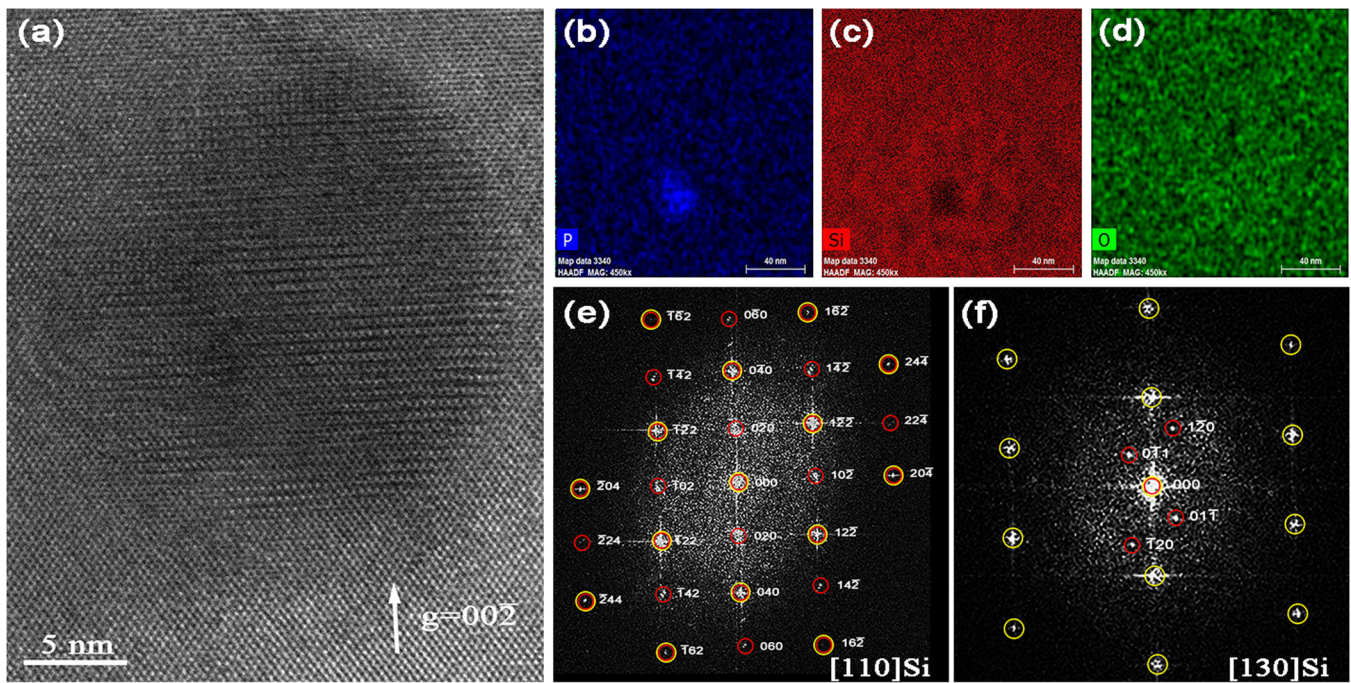


**FIG. 4.** (a) HRTEM image of a precipitate generated in the HP-CZ silicon specimen subjected to 950 °C/16 h anneal, (b)–(d) EDS areal mapping of P, Si, and O elements in the precipitate and silicon matrix, and (e) and (f) FFT diffraction patterns derived from the two HRTEM images of the SiP precipitate, taken along [110] and [130] orientations of the silicon matrix, respectively.

21 October 2023 10:19:51

and oxygen elements, as shown in Figs. 4(b) and 4(c), suggest that the precipitate is of SiP phase. Moreover, the FFT diffraction patterns shown in Figs. 4(e) and 4(f), derived from the two HRTEM images of the precipitate taken along [110] and [130] zone axes of silicon matrix, respectively, also indicate that the precipitate possesses an orthorhombic crystal structure. The inter-planar distances of the indexed planes shown in Figs. 4(e) and 4(f) are listed in Table III. Accordingly, the lattice parameters for the orthorhombic SiP precipitate are deduced as  $a = 6.81 \text{ \AA}$ ,  $b = 10.6 \text{ \AA}$ , and  $c = 8.19 \text{ \AA}$ . Furthermore, by analyzing the Miller indices of the diffraction spots listed in Table III, it is found that only the reflections of  $(hkl)$  with  $k+l \neq 2n$  ( $n$  is an integer) are absence, indicating that the crystal is of A-centered lattice.<sup>20</sup> Besides, the diffraction spot of

(011) excludes the “b” glide plane perpendicular to the a-axis and the diffraction spot of (102) excludes the “a” glide plane perpendicular to the b-axis, which further excludes the space groups of Abm2, Ama2, and Aba2. Thus, the space group of the SiP precipitates with an A-centered lattice can only be determined as Amm2.<sup>19</sup>

It should be mentioned that the FFT diffraction pattern (not shown herein) was also derived for each precipitate shown in Fig. 2. Except the diffraction spots belonging to the silicon matrix, the rest in the FFT diffraction pattern can be indexed into one of the aforementioned two orthorhombic SiP phases. Therefore, it is believed that the precipitate-like defects in HP-CZ silicon formed by the isothermal anneals at 450–1050 °C, as shown in Fig. 2, are essentially the SiP precipitates. Moreover, it is believed that tiny SiP precipitates can form during the crystal growth of HP-CZ silicon, as verified by the grown-in SiP precipitate shown in Fig. 2(j2). Actually, it should be pointed out that the orthorhombic SiP precipitates with the primitive and A-centered crystal lattices, respectively, are found to coexist in HP-CZ silicon annealed at 450–1050 °C for a sufficiently long time.

**TABLE III.** Interplanar distances of the indexed planes of the SiP precipitate shown in Figs. 4(e) and 4(f).

hkl	$d_o$ (Å)	hkl	$d_o$ (Å)
011	6.48	142	2.14
020	5.30	204	1.79
120	4.16	060	1.74
102	3.57	224	1.73
122	3.09	162	1.60
040	2.68	244	1.45

#### D. Effects of excess point defects on phosphorus precipitation

Figure 5 shows the areal densities of SiP precipitates formed in the HP-CZ silicon specimens subjected to 650–850 °C/32 h,

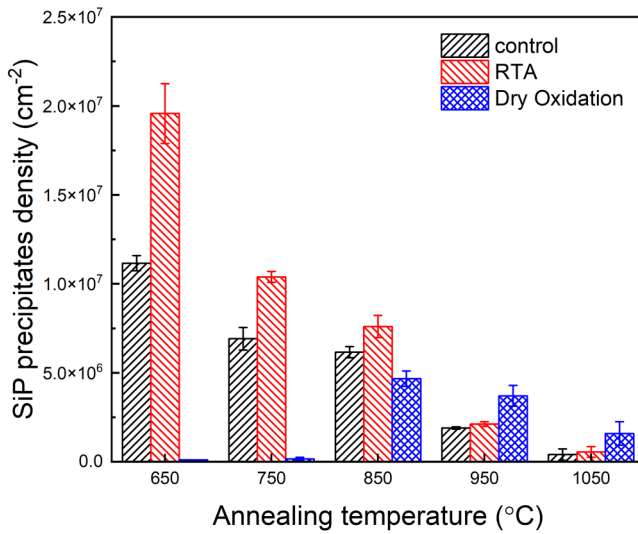
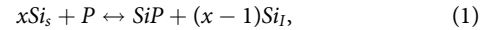


**FIG. 5.** Areal densities of SiP precipitates in the HP-CZ silicon specimens subjected to 650 °C/32 h, 750 °C/32 h, 850 °C/32 h, 950 °C/16 h, and 1050 °C/4 h anneals, respectively, with or without prior 1250 °C/60 s RTA in an Ar ambience or prior 1100 °C/4 h dry oxidation. Note that nearly no SiP precipitates are detected in the specimen annealed at 650 °C, following 1100 °C/4 h dry oxidation.

950 °C/16 h, and 1050 °C/4 h anneals, respectively, without and with prior 1250 °C/60 s RTA in an Ar ambience or prior 1100 °C/4 h dry oxidation. Herein, the average density of SiP precipitates was obtained by the measurements at six randomly selected regions on the preferentially etched planes of each annealed specimen. As can be seen, prior 1250 °C/60 s RTA remarkably enhances the formation of SiP precipitates by the isothermal anneal at 650–850 °C, while hardly affecting phosphorus precipitation at 950–1050 °C. Moreover, prior 1100 °C/4 h dry oxidation remarkably suppresses/enhances the formation of SiP precipitates by the isothermal anneal at 650–850 °C/950–1050 °C. Note that nearly no SiP precipitates were delineated in the specimen with the isothermal anneal at 650 °C, following the 1100 °C/4 h dry oxidation. It is well known that the 1250 °C/60 s RTA in an Ar ambience introduces vacancies, while oxidation at elevated temperatures substantially injects interstitial silicon ( $\text{Si}_I$ ) atoms into the silicon matrix.<sup>11–13</sup> Therefore, the results of Fig. 5 indicate that the presence of excess vacancies in HP-CZ silicon can enhance phosphorus precipitation at 650–850 °C but hardly affects that at 950–1050 °C, while the presence of excess  $\text{Si}_I$  atoms in HP-CZ silicon can suppress/enhance phosphorus precipitation at 650–850 °C/950–1050 °C. The mechanisms underlying the aforementioned effects of excess point defects on phosphorus precipitation in HP-CZ silicon will be elucidated in the following.

As already defined above, the SiP precipitates formed in HP-CZ silicon are crystalline in nature with the orthorhombic structure. Herein, it is believed that the mass density of SiP precipitates in HP-CZ silicon is roughly equal to that of free-standing orthorhombic SiP crystal, which was reported to be  $\sim 2.4 \text{ g/cm}^3$ .<sup>21</sup>

Then, it is calculated that the molar volume of the SiP precipitates is about twice that of the silicon matrix. In this context, the generation of SiP precipitates introduces compressive strain into the silicon matrix. In order to relieve such compressive strain, an amount of  $\text{Si}_I$  atoms should be ejected into the silicon matrix. Generally, the reaction equation for phosphorus precipitation in HP-CZ silicon can be expressed as follows:



where the subscripts of “*s*” and “*I*” denote the substitutional and interstitial sites, respectively. *x* represents the ratio between the molar volumes of the silicon matrix and SiP precipitates. A completely strain-free phosphorus precipitation requires *x* to reach the maximum value of  $\sim 2$ . In most cases, phosphorus precipitation is accompanied by the compressive strain. The effectiveness of relieving compressive strain affects the extent of phosphorus precipitation. Regarding how the phosphorus impurities diffuse toward the  $\text{Si}_s$  atoms with which react to form the SiP precipitates, either the vacancy or interstitialcy mechanism could predominantly operate, depending on either vacancies or  $\text{Si}_I$  atoms are abundant.

It should be noted that the HP-CZ silicon wafer used herein has an electron concentration of  $\sim 7.35 \times 10^{19} \text{ cm}^{-3}$ , which is much larger than the intrinsic carrier concentration in silicon at 1050 °C. Therefore, this HP-CZ silicon is always extrinsic at all the investigated temperatures. Then, according to the previous works,<sup>10,22,23</sup> the phosphorus diffusivity can be given by

$$D_P = h \left[ D_i^X + D_i^- \left( \frac{C_{V^-}}{C_{V^-}^i} \right) + D_i^= \left( \frac{C_{V^=}}{C_{V^=}^i} \right) \right], \quad (2)$$

where *h* is the self-electric-field enhancement factor;<sup>24</sup>  $D_i^X$ ,  $D_i^-$ , and  $D_i^=$  are respectively, the intrinsic phosphorus diffusivities due to pairing with the neutral, single-negatively, and double-negatively charged point defects;  $C_{V^-}$  and  $C_{V^=}$  are, respectively, the concentrations of vacancies in single-negative and double-negative charge states; and  $C_{V^-}^i$  and  $C_{V^=}^i$  are, respectively, the intrinsic concentrations of single- and double-negatively charged vacancies in silicon. Moreover,  $D_i^X$  is suggested to be primarily dictated by the interstitialcy mechanism.<sup>25,26</sup> Furthermore, it should be mentioned that phosphorus diffusion is believed to be much faster via the interstitialcy mechanism than via the vacancy mechanism,<sup>27</sup> namely,  $D_i^X \gg D_i^-$  and  $D_i^X \gg D_i^=$ . Thus, only when  $C_{V^-} \gg C_{V^-}^i$  or/and  $C_{V^=} \gg C_{V^=}^i$ , the second item or/and the third item in Eq. (2) can be greater than  $D_i^X$ . In this case, the vacancy mechanism is dominant in the phosphorus diffusion. On the other hand, if there are any excess  $\text{Si}_I$  atoms in the silicon matrix, the phosphorus diffusion will be dominated by the interstitialcy mechanism, and then, the phosphorus diffusivity does not follow Eq. (2). To understand the results of Fig. 5, one should keep in mind that the vacancy mechanism primarily dictates the phosphorus diffusion in the controls and in the specimens with prior RTA at 1250 °C, while the interstitialcy mechanism dominates the phosphorus diffusion in the specimens with prior dry oxidation at 1100 °C.

As for phosphorus precipitation in HP-CZ silicon at relatively low temperatures, i.e., 650–850 °C, it is seriously restricted by insufficient strain-relief, which is caused by the inefficient emission of

$\text{Si}_\text{l}$  atoms. For the specimens with prior RTA at 1250 °C, the additionally introduced vacancies provide spaces for relieving the strain arisen from phosphorus precipitation. Moreover, the effective phosphorus diffusivity is increased to a certain degree due to the additional vacancies, which can be derived according to Eq. (2). Such two positive factors enable phosphorus precipitation at 650–850 °C to be stronger in the specimens with prior RTA than in the controls, as shown in Fig. 5. By contrast, for the specimens with prior dry oxidation at 1100 °C, the large number of injected  $\text{Si}_\text{l}$  atoms form an environment for more difficult strain-relief at low temperatures, which is thermodynamically unfavorable for phosphorus precipitation. In other words, the forward reaction as indicated in Eq. (1) is more difficult to proceed in the presence of abundant  $\text{Si}_\text{l}$  atoms. Actually, Fig. 5 shows that the SiP precipitates are hardly generated at 650 and 750 °C in the specimens with prior dry oxidation. Moreover, phosphorus precipitation at 850 °C is distinctly weaker in the specimen with prior dry oxidation than in the control. Note that the phosphorus diffusion at 650–850 °C in the specimens with prior dry oxidation is principally via the interstitialcy mechanism and, thus, faster than that in the controls, which is primarily dictated by the vacancy mechanism. This positive effect on phosphorus precipitation, however, cannot offset the negative effect of the abundant  $\text{Si}_\text{l}$  atoms on phosphorus precipitation as mentioned above.

Regarding phosphorus precipitation in HP-CZ silicon at elevated temperatures, i.e., 950–1050 °C, the associated strain can be readily relieved because the ejection of  $\text{Si}_\text{l}$  atoms is efficient at such high temperatures. In this context, phosphorus precipitation is primarily controlled by the phosphorus diffusion. For the specimens with prior RTA at 1250 °C, according to Eq. (2), it is known that the enhancement effect of the additional vacancies on the phosphorus diffusivity is quite weak at 950–1050 °C since  $C_{V^-}$  or  $C_{V^=}$  is just a little bit larger than  $C_{V^-}^i$  or  $C_{V^=}^i$ , which is increased by orders of magnitude at 950–1050 °C with respect to that at 650–850 °C. Moreover, the marginal benefit of the additional vacancies for the strain-relief in phosphorus precipitation at 950–1050 °C becomes smaller. After all, the ejection of  $\text{Si}_\text{l}$  atoms at 950–1050 °C has been efficient enough for the strain-relief. In brief, the two positive effects of the RTA-introduced additional vacancies on phosphorus precipitation, as mentioned above, become much weaker at 950–1050 °C than at 650–850 °C. As a result, the enhanced phosphorus precipitation due to prior RTA is quite limited at 950–1050 °C, as can be seen from Fig. 5. However, for the specimens with prior dry oxidation at 1100 °C, the phosphorus diffusion at 950–1050 °C is significantly enhanced with respect to that in the controls by the large number of injected  $\text{Si}_\text{l}$  atoms via the interstitialcy mechanism. Consequently, phosphorus precipitation at 950–1050 °C is more significant in the specimens with prior dry oxidation than in the controls, as shown in Fig. 5. It is well known that thermal oxidation is usually a necessary process for device fabrication.<sup>11,28</sup> As mentioned earlier, the electrical deactivation of phosphorus impurities in HP-CZ silicon is not enabled by the anneal at 1100 °C and above. Thus, the oxidation temperature for the device fabrication is suggested to be no less than 1100 °C in order to hardly alter the electrical resistivity of the HP-CZ silicon substrate.

By the way, it is mentioned that although the effects of excess point defects on phosphorus precipitation at 450 or 550 °C have

not been investigated in Fig. 5, they can be logically derived according to the above analyses. Namely, phosphorus precipitation at 450 or 550 °C will be significantly enhanced by the RTA-introduced vacancies, and it will be almost inhibited by the excess  $\text{Si}_\text{l}$  atoms injected by the prior dry oxidation.

## E. Phosphorus solubilities in dislocation-free silicon

The phosphorus solubilities in silicon can be readily found in literature studies.<sup>10,29,30</sup> For example, the phosphorus solubility at 1250 °C is found to be  $\sim 1.1 \times 10^{21} \text{ cm}^{-3}$ .<sup>29</sup> However, such a high concentration of phosphorus impurities in silicon, generally acquired by the thermal diffusion or the ion implantation, always results in numerous dislocations.<sup>3,6</sup> It is known that the covalent radius of phosphorus atoms is ~6% smaller than that of silicon atoms.<sup>31</sup> Therefore, the doped phosphorus impurities bring about tensile stress in the silicon lattice. As the phosphorus concentration is considerably high (e.g.,  $10^{21} \text{ cm}^{-3}$ ), the lattice stress will be larger than the yield strength of silicon crystal, thus generating dislocations that can accommodate a number of impurities. Intuitively, the phosphorus solubilities in the dislocation-free silicon must be much smaller than the existing data. In this work, in order to derive the phosphorus solubilities in the dislocation-free silicon, which have never been reported previously, the critical temperatures, below or above which phosphorus precipitation occurs or not, have been approximately defined for a set of HP-CZ silicon wafers with the resistivities ranging from 1.01 to 3.91 mΩ cm, corresponding to the phosphorus concentrations decreasing from  $7.35 \times 10^{19}$  to  $1.55 \times 10^{19} \text{ cm}^{-3}$ . Herein, the specimens were subjected to the annealing schemes with different times of 4–128 h at temperatures ranging from 600 to 1100 °C with an interval of 50 °C, which are indicated in Table IV. Whether phosphorus precipitation occurs or not in each annealed specimen was successively judged through the change in the electron concentration derived by Hall effect measurements and through the preferential etching.

21 October 2023 10:19:51

**TABLE IV.** Occurrence or absence of phosphorus precipitation in a set of HP-CZ silicon specimens, with different phosphorus concentrations, subjected to different annealing schemes.

Annealing scheme	Phosphorus concentration ( $\times 10^{19} \text{ cm}^{-3}$ )						
	7.35	6.20	5.64	3.79	3.06	2.13	1.55
1100 °C/4 h	—	—	—	—	—	—	—
1050 °C/4 h	+	—	—	—	—	—	—
1000 °C/4 h	+	+	—	—	—	—	—
950 °C/16 h	+	+	+	—	—	—	—
900 °C/32 h	+	+	+	—	—	—	—
850 °C/32 h	+	+	+	+	—	—	—
800 °C/32 h	+	+	+	+	+	—	—
750 °C/64 h	+	+	+	+	+	—	—
700 °C/64 h	+	+	+	+	+	—	—
650 °C/128 h	+	+	+	+	+	+	—
600 °C/128 h	+	+	+	+	+	+	+

Note: The symbols “+” and “−” represent the occurrence and absence of phosphorus precipitation, respectively.

In Table IV, the symbols “+” and “–” represent the occurrence and absence of phosphorus precipitation, respectively.

As illustrated in Table IV, the maximum annealing temperature (in terms of the temperatures adopted in this work), at which phosphorus precipitation can still occur in HP-CZ silicon, decreases with the decreasing phosphorus concentration. For example, the maximum annealing temperature is 1050 °C for the phosphorus concentration of  $7.35 \times 10^{19} \text{ cm}^{-3}$ , while it is lowered to 600 °C as the phosphorus concentration decreases to  $1.55 \times 10^{19} \text{ cm}^{-3}$ . Essentially, the aforementioned maximum annealing temperature decreases with the decreasing supersaturation of phosphorus impurities. Based on the result of Table IV, Fig. 6 shows the maximum temperature (marked by the blue block) at which phosphorus precipitation can still occur and the minimum temperature (marked by the red circle) at which phosphorus precipitation is absent for each investigated phosphorus concentration in HP-CZ silicon. Understandably, the solvus line for the phosphorus impurities in silicon must lie in between the blue blocks and the red circles shown in Fig. 6. By virtue of the open-access PanPhaseDiagram and PanOptimizer modules in PANDAT software based on the CALPHAD method,<sup>32,33</sup> the solvus line for the phosphorus impurities in silicon in the temperature range of 600–1100 °C can be automatically derived by inputting the phosphorus concentrations and their corresponding maximum and minimum temperatures, as shown in Fig. 6. Furthermore, the derived solvus line, as depicted with the black

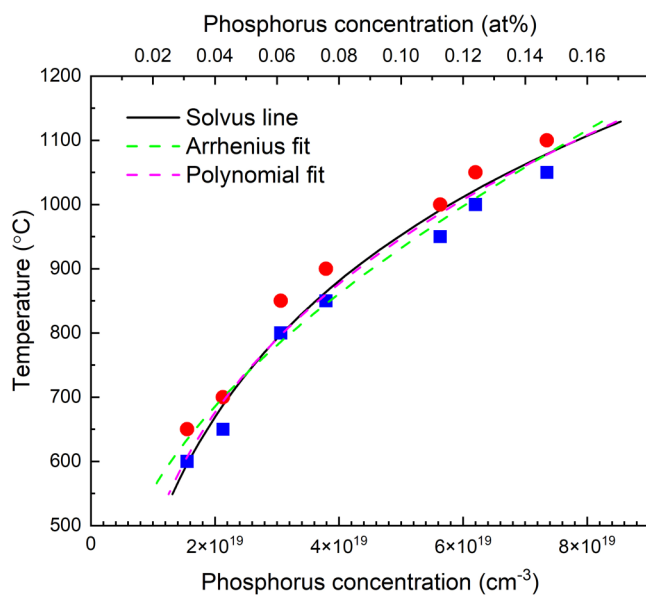


**FIG. 6.** The maximum temperature (marked by the blue block) at which phosphorus precipitation can still occur and the minimum temperature (marked by the red circle) at which phosphorus precipitation is absent for each investigated phosphorus concentration in HP-CZ silicon. The black solid curve, fitted by the CALPHAD method, represents the solvus line for the phosphorus impurities in silicon. The green and pink dashed curves are used to fit the solvus line according to Eqs. (3) and (4), respectively.

solid curve in Fig. 6, can be fitted by the following two equations manifested with Arrhenius and polynomial expressions, respectively:

$$C_s = 1.756 \times 10^{21} \exp(-0.37 \text{ eV}/kT)(\text{cm}^{-3}), \quad (3)$$

$$C_s = 3.940 \times 10^{17} + 2.211 \times 10^{16}T - 4.405 \times 10^{13}T^2 + 8.024 \times 10^{10}T^3(\text{cm}^{-3}). \quad (4)$$

As can be seen from Fig. 6, the Arrhenius expression [Eq. (3)] can be used to fit the solvus line quite well. By comparison, the fitted line via the polynomial expression [Eq. (4)] is more consistent with the solvus line. Therefore, the fitting of the solvus line by Eq. (4) is reasonable to be preferred in this work, hereafter. Actually, the polynomial expressions were usually used to fit the solvus lines for other solutions.<sup>34–36</sup> According to Eq. (4), the phosphorus solubility in the dislocation-free silicon at 1100 °C is calculated to be  $7.82 \times 10^{19} \text{ cm}^{-3}$ , which is quite close to the experimentally derived value of  $\sim 8.2 \times 10^{19} \text{ cm}^{-3}$  in the work of Chiou.<sup>1</sup> Therefore, Eq. (4) may be used to express the dependence of phosphorus solubility in the dislocation-free silicon on the temperature. It should be pointed out that Eq. (4) cannot be extrapolated to the temperatures above the melting point of the SiP phase, which is reported to be 1131 °C.<sup>16</sup> From the perspective of the existing phase diagram of the Si-P binary system, the solvus line in the extremely silicon-rich region is absent. Of significance, this issue can be settled by incorporating the solvus line shown in Fig. 6 into the existing phase diagram of the Si-P binary system. Moreover, the finding of phosphorus solubilities at different temperatures in the dislocation-free silicon provides the basis to derive the minimum resistivity (the highest phosphorus concentration), which can be achieved for the dislocation-free HP-CZ silicon and to understand the phosphorus precipitation behavior in HP-CZ silicon.

## F. Thermodynamics analysis on nucleation for phosphorus precipitation

As shown in Fig. 2, phosphorus precipitation can occur in HP-CZ silicon subjected to different anneals at appropriate temperatures. This precipitation process can be expressed as



where  $Si_0$  represents the solid solution containing a high concentration of phosphorus impurities, which is thermodynamically stable at sufficiently high temperatures. At a low enough temperature,  $Si_0$  will decompose into the SiP precipitates and  $Si_1$  solid solution containing a decreased concentration of phosphorus impurities. According to the classical thermodynamical theory,<sup>37–39</sup> the change in the total free energy ( $\Delta G$ ) due to the phosphorus precipitation can be expressed as

$$\Delta G = -V\Delta G_v + V\Delta G_s + A\gamma, \quad (6)$$

where  $V$  is the volume of SiP precipitate,  $\Delta G_v$  is the decrease in the free energy per unit volume,  $\Delta G_s$  is the increase in the strain energy

per unit volume,  $A$  is the area of the interface between the SiP precipitate and the silicon matrix, and  $\gamma$  is the interface energy per unit area.

$\Delta G_v$  in Eq. (6) can be derived from

$$\Delta G_v = \frac{\Delta G_N}{V_{SiP}}. \quad (7)$$

According to the classical phase transformation theory,<sup>38</sup> we have

$$\Delta G_N = \left( (0.5 - x_p) \frac{\partial G_{Si,P}}{\partial x} |_{x=x_p} + G_{Si,P} |_{x=x_p} \right) - G_{SiP}, \quad (8)$$

where  $\Delta G_N$  is the decrease in the free energy due to phosphorus precipitation,  $V_{SiP}$  is the molar volume of the SiP precipitate,  $x_p$  is the atomic percentage of phosphorus impurities in silicon,  $G_{Si,P}$  is the Gibbs free energy of silicon solid solution containing phosphorus impurities, and  $G_{SiP}$  is the Gibbs free energy of the SiP precipitate. Herein,  $G_{Si,P}$  and  $G_{SiP}$  can be derived by using the aforementioned CALPHAD method, and they are expressed as

$$G_{SiP} = -78014.8 + 224.656T - 38.343T\ln T - 0.00544T^2 + 282500T^{-1}, \quad (9)$$

$$G_{Si,P} = x_p G_p + (1 - x_p) G_{Si} + RT [x_p \ln x_p + (1 - x_p) \ln(1 - x_p)] + x_p (1 - x_p) [-58562.4 + 38.9825T + 5.33285T\ln(T) - 0.02271604T^2 - 40009.59989T^{-1}], \quad (10)$$

where  $R$  is the gas constant, and  $G_{Si}$  and  $G_p$  are, respectively, the Gibbs free energies of the silicon matrix and phosphorus impurities, which can be found in the SGTE database.<sup>40</sup>

Based on the work of Nabarro,<sup>41</sup>  $\Delta G_s$  in Eq. (6) can be derived from

$$\Delta G_s = \frac{6\mu}{1 + \frac{4\mu}{3K}} \delta^2 \Omega_{Si} f, \quad (11)$$

where  $\mu = 79.5$  GPa and  $K = 97.8$  GPa,<sup>42–44</sup> being the shear and bulk moduli of silicon, respectively,  $\delta$  is the linear misfit between the SiP precipitate and silicon matrix, and  $f$  is a parameter related to the shape of the precipitate, lying between 0 and 1 (for the sphere-like precipitate,  $f = 1$ ). Furthermore, the linear misfit strain,  $\delta$ , can be derived from

$$\delta = \left( \frac{\Omega_{SiP}}{\Omega_{Si}} \right)^{\frac{1}{3}} - 1, \quad (12)$$

where  $\Omega_{Si}$  is the volume per Si atom in the matrix and  $\Omega_{SiP}$  is the volume per Si atom in the SiP precipitate.

The interface energy per unit area,  $\gamma$ , in Eq. (6) can be estimated through Generalized broken-bond (GBB) method.<sup>45,46</sup> Then,

we have

$$\gamma = \frac{n_s Z_{S,eff}}{N_A Z_{L,eff}} \Delta H_{sol}, \quad (13)$$

where  $n_s$  is the number of atoms in a unit interface area and  $n_s = 4^{2/3}/a^2$  for the face-centered-cubic (fcc) crystal structure, in which  $a$  represents the lattice constant of silicon,  $N_A$  is the Avogadro constant, and  $Z_{S,eff}$  and  $Z_{L,eff}$  represent the effective numbers of the broken bonds and covalent bonds, respectively, per atom at the interface. Since silicon is of fcc crystal structure, the structural factor  $Z_{S,eff}/Z_{L,eff}$  is equal to 0.329.<sup>45</sup>  $\Delta H_{sol}$  is the change in the enthalpy for precipitating one mole of SiP out of the silicon matrix, which can be calculated from

$$\Delta H_{sol}(T) = \left( G_{Si,P} - T \frac{\partial G_{Si,P}}{\partial T} \right) - H_{sol}(298 \text{ K}). \quad (14)$$

Figure 7 shows the calculated temperature-dependent interface energy for the formation of SiP precipitates in the HP-CZ silicon with a phosphorus concentration of  $7.35 \times 10^{19} \text{ cm}^{-3}$ . As can be seen, the interface energy per unit area increases with the annealing temperature for the formation of SiP precipitates.

In order to conveniently evaluate the critical radius ( $r_c$ ) and the steady-state nucleation rate ( $J$ ) for phosphorus precipitation in HP-CZ silicon, it is supposed that phosphorus precipitation is dictated by homogeneous nucleation and the resulting SiP precipitates are sphere-like. Then, Eq. (6) is translated as

$$\Delta G = -\frac{4}{3}\pi r^3 (\Delta G_v - \Delta G_s) + 4\pi r^2 \gamma. \quad (15)$$

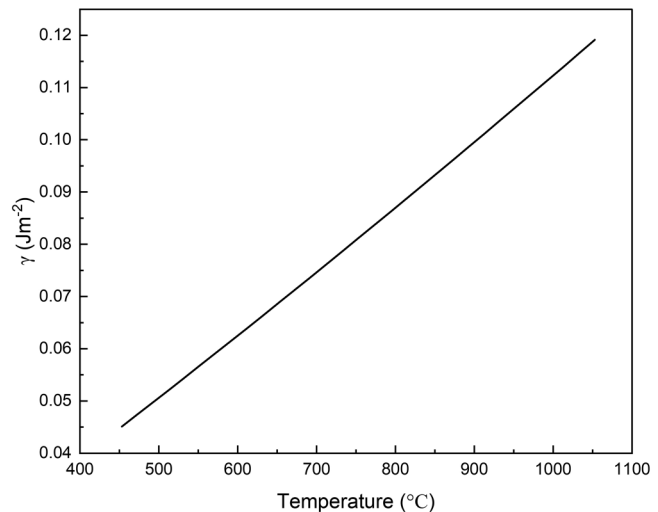


FIG. 7. Temperature-dependent interface energy per unit area for the formation of SiP precipitates in HP-CZ silicon with a phosphorus concentration of  $7.35 \times 10^{19} \text{ cm}^{-3}$ .

Accordingly, the critical radius ( $r_c$ ) and the corresponding critical nucleation barrier ( $\Delta G_c$ ) can be derived from Eq. (15) as

$$r_c = \frac{2\gamma}{\Delta G_v - \Delta G_s}, \quad (16)$$

$$\Delta G_c = \frac{16\pi\gamma^3}{3(\Delta G_v - \Delta G_s)^2}. \quad (17)$$

Furthermore, the steady-state nucleation rate,  $J$ , for phosphorus precipitation based on the classical nucleation theory can be expressed as<sup>37</sup>

$$J = Z\beta^* N_0 \exp\left(-\frac{\Delta G_c}{kT}\right), \quad (18)$$

where  $N_0$  is the number of the nucleation sites,  $k$  is the Boltzmann constant,  $Z$  is the Zeldovich factor, and  $\beta^*$  is the frequency of phosphorus atoms sticking to a critical nucleus. Moreover,  $Z$  and  $\beta^*$  can be derived from Refs. 47 and 48,

$$Z = \frac{V_{Si}}{2\pi N_A r_c^2} \sqrt{\frac{\gamma}{kT}} \quad (19)$$

$$\beta^* = \frac{4\pi r_c^2}{a^4 \Omega_{Si}} \left[ \frac{(C_p - C_0)^2}{C_0 D_p} \right]^{-1}, \quad (20)$$

where  $C_p$  and  $C_0$  are, respectively, the concentrations of

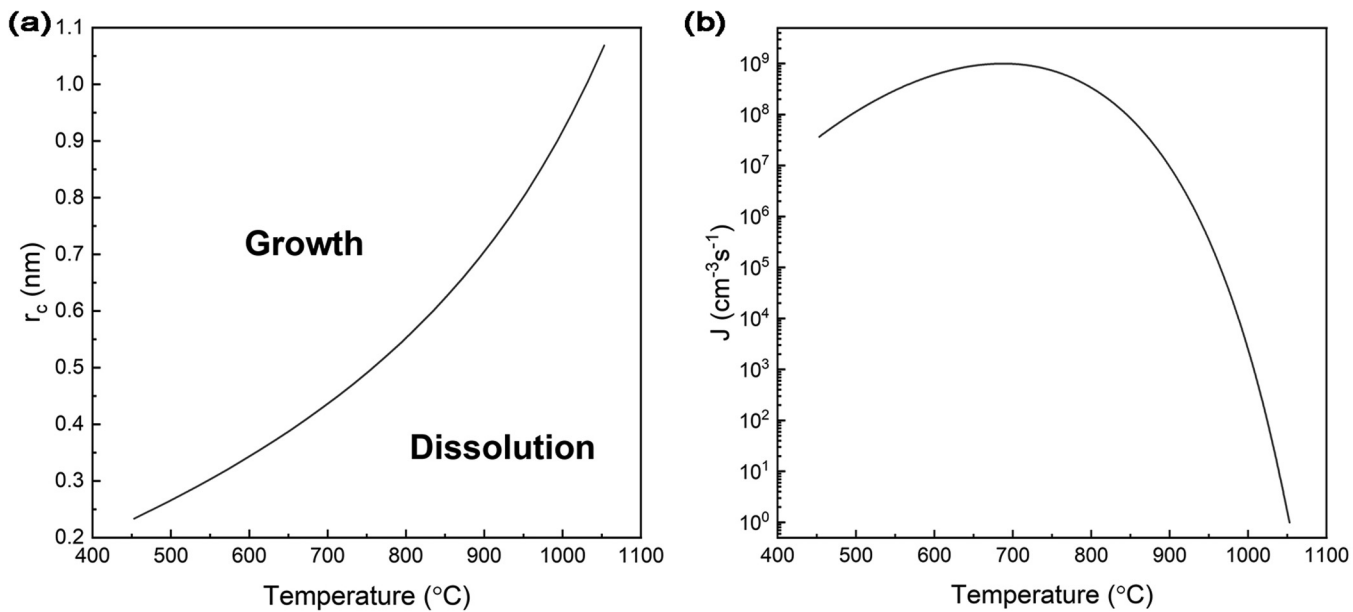
phosphorus impurities in the SiP precipitate and the silicon matrix, and  $D_p$  is the phosphorus diffusivity at a given temperature.

Combining Eq. (16) with Eqs. (7)–(14), one gets the dependence of the critical radius for phosphorus precipitation on the annealing temperature, as illustrated in Fig. 8(a). It is evident that the critical radius increases constantly with the annealing temperature. Moreover, combining Eq. (18) with Eqs. (7)–(14), (17), (19), and (20), one obtains the dependence of the steady-state nucleation rate for phosphorus precipitation on the annealing temperature, as shown in Fig. 8(b). Herein, the phosphorus diffusivities are referred to the previous works.<sup>10,22,25</sup> As can be seen, the steady-state nucleation rate remains considerably high in the temperature range of 450–850 °C and then drops rapidly with increasing temperature. Returning to Fig. 2, one can see considerably dense etching pits related to the SiP precipitates formed in the specimens annealed at 450–850 °C. However, the etching pit density in the specimen annealed at 950 °C decreases remarkably and that in the specimens respectively annealed at 1000 and 1050 °C is quite low. Such experimental results can be qualitatively understood according to the theoretical results as just mentioned above.

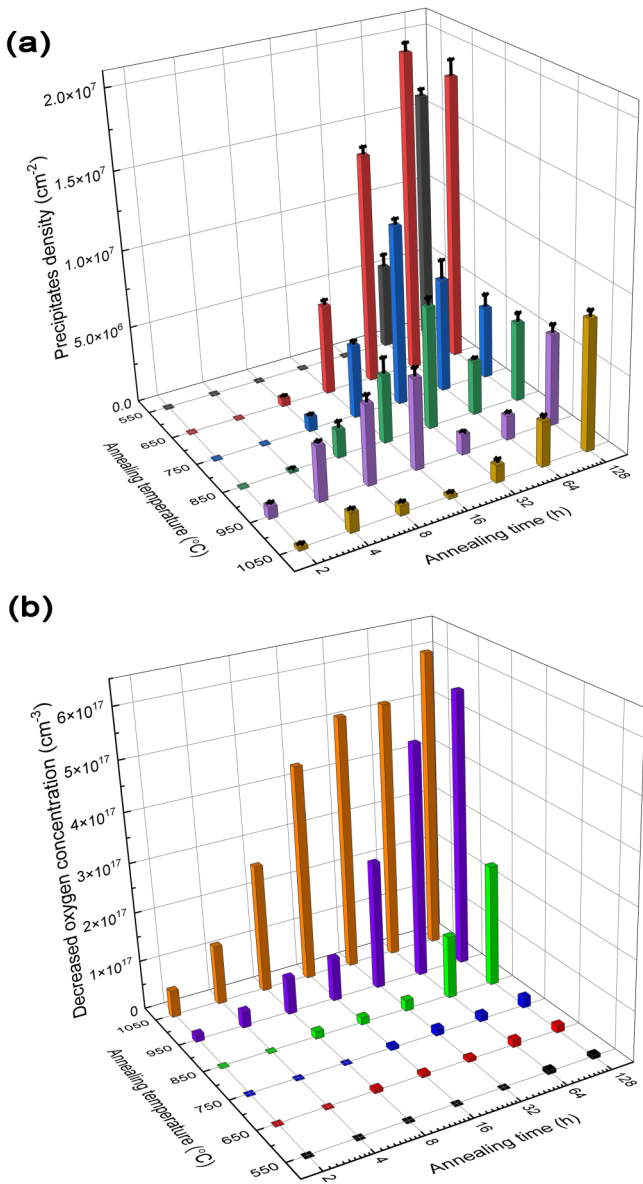
## G. Kinetics of phosphorus precipitation

Figure 9(a) shows the evolutions of the areal density of precipitates formed in the HP-CZ silicon specimens, annealed at 550–1050 °C in 100 °C increments, with the annealing time up to 128 h. Herein, the average density of precipitates was also obtained by the measurements at six randomly selected regions on the preferentially etched planes of each annealed specimen. In principle, the precipitates formed in the HP-CZ silicon specimens may

21 October 2023 10:19:51



**FIG. 8.** (a) Critical radius and (b) steady-state nucleation rate as a function of temperature for phosphorus precipitation in HP-CZ silicon with a phosphorus concentration of  $7.35 \times 10^{19} \text{ cm}^{-3}$ .



**FIG. 9.** (a) Evolutions of the areal precipitate density with the annealing time for the HP-CZ silicon specimens annealed at 550–1050 °C and (b) evolutions of the decreased oxygen concentration with the annealing time for the LP-CZ silicon specimens annealed at 550–1050 °C. Note that the direction of increasing temperature in (a) is the reverse of that in (b).

consist of the SiP and  $\text{SiO}_x$  precipitates, and which kinds of precipitates are predominant depends on the annealing temperature and time. Considering that oxygen precipitation in HP-CZ silicon cannot be conveniently characterized by using Fourier transformation infrared (FTIR) spectroscopy because of the strong optical absorption in the IR region by the high concentration of carriers,<sup>49,50</sup> we investigated oxygen precipitation in terms of the

reduction in the oxygen concentration measured by means of FTIR spectroscopy for a lightly phosphorus-doped CZ (LP-CZ) silicon, in which the oxygen concentration ( $7.73 \times 10^{17} \text{ cm}^{-3}$ ) was comparable with that in HP-CZ silicon ( $7.79 \times 10^{17} \text{ cm}^{-3}$ ). As a result, Fig. 9(b) shows the dependences of the decreased oxygen concentration on the annealing time up to 128 h for the LP-CZ silicon specimens annealed at 550–1050 °C in 100 °C increments. Although the scenario of oxygen precipitation in HP-CZ silicon cannot be the same as that in LP-CZ silicon, the results shown in Fig. 9(b) can be referred to estimate the extent of oxygen precipitation in HP-CZ silicon. After all, the supersaturations of oxygen impurities in LP- and HP-CZ silicon, which are the driving force for oxygen precipitation, are comparable. As shown in Fig. 9(b), the decreased oxygen concentration and, therefore, oxygen precipitation are quite slight in the case of anneal at 550, 650, or 750 °C. Then, the precipitate densities in the HP-CZ silicon specimens annealed at 550–750 °C, as shown in Fig. 9(a), can be approximately assigned to the SiP precipitate densities. When annealed at higher temperatures, oxygen precipitation in HP-CZ silicon could substantially occur upon sufficiently long annealing time, e.g., 64 h at 850 °C, 32 h at 950 °C, and 8 h at 1050 °C, as can be derived from Fig. 9(b). It is known that oxygen precipitation is accompanied by ejecting  $\text{Si}_l$  atoms into the silicon matrix.<sup>50</sup> Such ejected  $\text{Si}_l$  atoms with high enough concentration, according to Eq. (1), could enable the backward reaction to proceed at a given temperature, thus making the existing SiP precipitates be dissolved. Therefore, the occurrence of pronounced oxygen precipitation in HP-CZ silicon is unfavorable for the survival of SiP precipitates. Combining Figs. 9(a) and 9(b), the phenomenological analyses on the kinetics of phosphorus precipitation in HP-CZ silicon are tentatively described as follows:

- (1) In the case of the isothermal anneal at 550, 650, or 750 °C, as mentioned above, phosphorus precipitation is hardly affected by oxygen precipitation. As can be seen, there is an incubation period for the remarkable increase in the SiP precipitate density at each aforementioned temperature, indicating that the nucleation of SiP precipitates is limited by the diffusion of phosphorus impurities. It is worth noting that in the case of isothermal anneal at 750 °C, the SiP precipitate density peaks at the annealing time of 32 h and then decreases remarkably along with the annealing time up to 128 h. Moreover, in the case of isothermal anneal at 650 °C, the SiP precipitate density decreases a little as the annealing time is prolonged from 64 to 128 h. Such decreases in the SiP precipitate density are believed to be caused by the so-called Ostwald ripening effect, due to which the large-sized precipitates become further coarsened through swallowing up the small-sized ones.
- (2) In the case of the isothermal anneal at 850 °C, since oxygen precipitation is considerably slight during the first 32 h anneal, the precipitate density in Fig. 9(a) primarily represents the SiP precipitate density, which increases rapidly at the annealing time of 8 h and peaks at the annealing time of 32 h. With the annealing time prolonged to 64 h, oxygen precipitation becomes significant, leading to the dissolution of the existing SiP precipitates and, therefore, the obvious decrease in the SiP precipitate density. Moreover, such a decrease in the SiP precipitate density may also be partly caused by the Ostwald

ripening effect. As the annealing time is further prolonged to 128 h, which results in more significant oxygen precipitation, the precipitate density does not further decrease but increases instead. This is because the formed  $\text{SiO}_x$  precipitates are much more than the dissolved SiP precipitates.

- (3) In the case of the isothermal anneal at 950 °C, oxygen precipitation during the first 16 h annealing is not too obvious. Therefore, the formed precipitates are mostly SiP precipitates, with the density increasing constantly and peaking at the annealing time of 16 h. With the extension of annealing time from 16 to 128 h, oxygen precipitation becomes increasingly pronounced. In this context, more and more SiP precipitates are dissolved, driven by the supersaturation of  $\text{Si}_1$  atoms generated by the pronounced oxygen precipitation. As shown in Fig. 9(a), the precipitate density is remarkably decreased at the annealing time of 32 or 64 h, suggesting that the  $\text{SiO}_x$  precipitates formed by the prolonged anneal for 32 or 64 h are much fewer than the dissolved SiP precipitates. However, the precipitate density increases dramatically at the annealing time of 128 h, which is due to the occurrence of very pronounced oxygen precipitation. In this case, the  $\text{SiO}_x$  precipitates contribute to the majority of detected precipitate density.
- (4) In the case of the isothermal anneal at 1050 °C, the reason for the evolution of the precipitate density along with the annealing time is similar to that in the case of the isothermal anneal at 950 °C. The SiP precipitates form a peak density at the annealing time of 4 h and are then substantially dissolved at the annealing time of 16 h due to the occurrence of pronounced oxygen precipitation. With the prolonged anneal for 32 h and above, the precipitate density increases constantly, which is substantially contributed by the formed  $\text{SiO}_x$  precipitates.

It should be stated that although the above phenomenological analyses are by and large self-consistent, how oxygen precipitation genuinely affects phosphorus precipitation is yet to be essentially revealed. Moreover, why phosphorus precipitation seems to occur prior to oxygen precipitation and whether the SiP precipitates can act as the heterogeneous nucleation centers for oxygen precipitation need to be answered in further work.

To quantitatively understand the kinetics of phosphorus precipitation in HP-CZ silicon, based on Ham's theory of diffusion-limited precipitation,<sup>51</sup> we can attempt to derive a growth law in terms of the phosphorus precipitate density as a function of annealing time at a given temperature, expresses as

$$N(t) = N(\infty) \left[ 1 - \exp \left( -\frac{t - t_d}{t_p} \right) \right], \quad (21)$$

where  $N(t)$  represents the time-dependent density of phosphorus precipitates,  $N(\infty)$  represents the saturated density of phosphorus precipitates,  $t_d$  represents the nucleation time for phosphorus precipitation, and  $t_p$  is a best-fit time constant. Figure 10 shows the phosphorus precipitate density as a function of annealing time and temperature for the HP-CZ silicon specimens used in Fig. 9(a). As shown in Fig. 9(a), when annealed at 850–1050 °C, the extended annealing times lead to a decrease in the phosphorus precipitate density. Therefore, the data of 850, 950, and 1050 °C are taken with

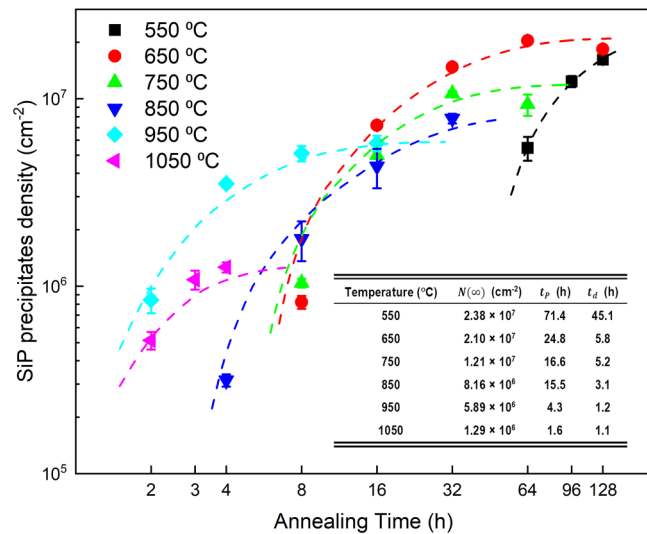


FIG. 10. Phosphorus precipitate density as a function of annealing time and temperature for the HP-CZ silicon specimens used in Fig. 9. The data of each annealing temperature are fitted with the dashed curve according to Eq. (21). The inset table lists the fitting parameters in Eq. (21) for each annealing temperature.

the upper-limit times of 32, 16, and 4 h, respectively. As can be seen from Fig. 10, the phosphorus precipitate density as a function of annealing time at each annealing temperature can be fitted by Eq. (21) to a large extent. The lower right inset in Fig. 10 shows the table where the fitting parameters of  $N(\infty)$ ,  $t_d$ , and  $t_p$  in Eq. (21) are listed for each annealing temperature. Special attention is paid to the nucleation time,  $t_d$ , which decreases dramatically with the increase in the annealing temperature. Understandably, the nucleation of phosphorus precipitates is expedited at a higher temperature, which is associated with a larger phosphorus diffusivity.

## H. Analysis of the SiP precipitate morphology

Figure 2 demonstrates that the morphology of the SiP precipitate in HP-CZ silicon exhibits a salient feature of depending on the annealing temperature. Roughly, three temperature regimes may be distinguished. The SiP precipitates take the platelet shape up to about 650 °C. From about 750 to 850 °C, the SiP precipitates exhibit the shape of a polyhedron. Moreover, the SiP precipitates are more and more inclined to be sphere-like shape with increasing temperature from 950 to 1050 °C. From the Gibbs free energy point of view, the SiP precipitates will take the shape with the free energy as low as possible. According to Eq. (6), the formation of a SiP precipitate, on one hand, brings about a reduced energy ( $-V\Delta G_v$ ); on the other hand, it leads to two items of increased energies, i.e., strain energy ( $V\Delta G_s$ ) and interface energy ( $A\gamma$ ). In principle, the strain energy is largest for the spherical shape and is smallest for the platelet shape, while the interface energy is smallest for the spherical shape and is largest for the platelet shape. At the low temperatures of 450–650 °C, there is little emission of  $\text{Si}_1$  atoms

to relieve the strain associated with phosphorus precipitation. Thus, the strain energy matters. In this case, the SiP precipitates tend to adopt a platelet shape with a certain thickness, with which the interface energy is much smaller than that in the case of “ideal platelet” with the smallest thickness of the order of the atomic dimension.<sup>52</sup> At the elevated temperatures of 950–1050 °C, the emission of Si<sub>1</sub> atoms becomes quite efficient for generating substantially strain-free SiP precipitates. Moreover, as shown in Fig. 7, the interface energy related to the SiP precipitates increases significantly at higher temperatures. Under these circumstances, the interface energy should be put on the agenda for the energy minimization. Then, the SiP precipitates are inclined to be sphere-like to achieve the least interface energy. In the intermediate temperature regime of 750–850 °C, the extent of strain-relief lies in between those of the low and the elevated temperature regimes. Thus, the SiP precipitates adopt the polyhedral shapes, in between the platelet and sphere-like shapes. Since the interface energy is anisotropy and exhibits a minimum on the {111} planes of silicon, as can be seen from Fig. 2, the polyhedral precipitates have several {111} bounding planes.

#### IV. CONCLUSIONS

In summary, we have intensively investigated phosphorus precipitation in HP-CZ silicon sufficiently annealed at 450–1050 °C. For HP-CZ silicon with a phosphorus concentration of  $\sim 7.35 \times 10^{19} \text{ cm}^{-3}$ , phosphorus precipitation can occur at temperatures even up to 1050 °C, which leads to the electrical deactivation of a fraction of doped phosphorus impurities. Through systematic TEM characterizations, it is found that the precipitates formed at each investigated temperature can be designated to be of the orthorhombic SiP phase, with two possible sets of lattice parameters:  $a = 6.47 \text{ \AA}$ ,  $b = 9.35 \text{ \AA}$ , and  $c = 7.56 \text{ \AA}$  (primitive crystal lattice) and  $a = 6.81 \text{ \AA}$ ,  $b = 10.6 \text{ \AA}$ , and  $c = 8.19 \text{ \AA}$  (A-centered crystal lattice). With the increase in the annealing temperature, the resultant SiP precipitates tend to adopt the platelet shape (450–650 °C), polyhedral shape (750–850 °C), and sphere-like shape (950–1050 °C), which makes the total free energy as small as possible. Regarding the effects of excess point defects on phosphorus precipitation in HP-CZ silicon, the excess vacancies enhance phosphorus precipitation significantly at temperatures no more than 850 °C and little affect that at higher temperatures, while the excess Si<sub>1</sub> atoms remarkably promote phosphorus precipitation at 950–1050 °C and almost completely suppress that at temperatures 750 °C and below. Such results can be understood in terms of the effects of point defects on the strain-relief and phosphorus diffusivity, which are the two crucial factors affecting phosphorus precipitation. In order to understand the nucleation for phosphorus precipitation, a rigorous thermodynamical analysis has been carried out based on the classical nucleation theory and the derived results can well account for the experimental phenomena in terms of the formed SiP precipitate densities. The kinetics of phosphorus precipitation occurring at different temperatures has been investigated, providing insight into the nucleation, growth, and dissolution of SiP precipitates. Addressing the fact that no data of phosphorus solubilities in the dislocation-free silicon crystal have yet been available, the solvus line for the phosphorus impurities in silicon in the

temperature range of 600–1100 °C is obtained by using PanPhaseDiagram and PanOptimizer modules in Pandat software, based on investigating the phosphorus precipitation behaviors in a set of HP-CZ silicon wafers with different phosphorus concentrations. Then, an empirical formula for the temperature-dependent phosphorus solubilities in the dislocation-free silicon has been derived. Moreover, the aforementioned solvus line is believed to be a beneficial supplement to the existing phase diagram of the Si-P binary system in the extremely silicon-rich corner. In a word, it is believed that this work has presented a comprehensive overall picture of phosphorus precipitation in HP-CZ silicon.

#### ACKNOWLEDGMENTS

This work was supported by the Natural Science Foundation of China (Grant Nos. 62174145, 51532007, and 61721005) and the Zhejiang Provincial Key R&D project (Grant No. 2020C01009).

#### AUTHOR DECLARATIONS

##### Conflict of Interest

The authors have no conflicts to disclose.

##### Author Contributions

Defan Wu and Tong Zhao equally contributed to this work.

**Defan Wu:** Data curation (lead); Formal analysis (equal); Methodology (lead); Visualization (equal); Writing – original draft (equal). **Tong Zhao:** Data curation (lead); Formal analysis (equal); Methodology (lead); Validation (lead); Visualization (lead); Writing – original draft (equal). **Bin Ye:** Data curation (supporting); Resources (equal); Validation (equal). **Hao Chen:** Data curation (supporting); Validation (equal). **Xingbo Liang:** Data curation (equal); Resources (equal). **Shenzhong Li:** Data curation (supporting); Resources (equal); Validation (equal). **Daxi Tian:** Data curation (supporting); Resources (equal). **Deren Yang:** Resources (lead); Supervision (lead). **Xiangyang Ma:** Conceptualization (lead); Resources (lead); Supervision (lead); Writing – review & editing (lead).

#### DATA AVAILABILITY

The data that support the findings of this study are available from the corresponding author upon reasonable request.

#### REFERENCES

- <sup>1</sup>H.-D. Chiou, *J. Electrochem. Soc.* **147**(1), 345 (2000).
- <sup>2</sup>P. Ostoja, D. Nobili, A. Armigliato, and R. Angelucci, *J. Electrochem. Soc.* **123**(1), 124–129 (1976).
- <sup>3</sup>Y. Zeng, X. Ma, D. Tian, W. Wang, L. Gong, D. Yang, and D. Que, *J. Appl. Phys.* **105**(9), 093503 (2009).
- <sup>4</sup>C. G. Beck and R. Stickler, *J. Appl. Phys.* **37**(13), 4683–4687 (1966).
- <sup>5</sup>M. Servidori and A. Armigliato, *J. Mater. Sci.* **10**(2), 306–313 (1975).
- <sup>6</sup>H. Bender, A. De Veirman, J. Van Landuyt, and S. Amelinckx, *Appl. Phys. A: Solids Surf.* **39**(2), 83–90 (1986).
- <sup>7</sup>S. Solmi and D. Nobili, *J. Appl. Phys.* **83**(5), 2484–2490 (1998).
- <sup>8</sup>S. Solmi, A. Parisini, R. Angelucci, A. Armigliato, D. Nobili, and L. Moro, *Phys. Rev. B* **53**(12), 7836–7841 (1996).

- <sup>9</sup>D. Nobili, A. Armigliato, M. Finnetti, and S. Solmi, *J. Appl. Phys.* **53**(3), 1484–1491 (1982).
- <sup>10</sup>P. Pichler, *Intrinsic Point Defects, Impurities, and Their Diffusion in Silicon* (Springer Science & Business Media, Berlin, 2012), pp. 390–404.
- <sup>11</sup>K. Taniguchi, Y. Shibata, and C. Hamaguchi, *J. Appl. Phys.* **65**(7), 2723–2727 (1989).
- <sup>12</sup>M. Pagani, R. J. Falster, G. R. Fisher, G. C. Ferrero, and M. Olmo, *Appl. Phys. Lett.* **70**(12), 1572–1574 (1997).
- <sup>13</sup>X. Zhang, C. Gao, M. Fu, X. Ma, J. Vanhellemont, and D. Yang, *J. Appl. Phys.* **113**(16), 163510 (2013).
- <sup>14</sup>L. J. van der Pauw, Philips Res. Rep. **13**(1), 1 (1958).
- <sup>15</sup>K. H. Yang, *J. Electrochem. Soc.* **131**(5), 1140–1145 (1984).
- <sup>16</sup>R. W. Olesinski, N. Kanani, and G. J. Abbaschian, *Bull. Alloy Phase Diagrams* **6**(2), 130–133 (1985).
- <sup>17</sup>P. F. Schmidt and R. Stickler, *J. Electrochem. Soc.* **111**(10), 1188 (1964).
- <sup>18</sup>J. Osugi, K. Shimizu, and Y. Tanaka, *Proc. Jpn. Acad.* **85**(3), 183 (1966).
- <sup>19</sup>D. W. Bennett, *Understanding Single-Crystal X-ray Crystallography* (John Wiley & Sons, New York, 2010), pp. 195–275.
- <sup>20</sup>B. Fultz and J. M. Howe, *Transmission Electron Microscopy and Diffractometry of Materials* (Springer Science & Business Media, Berlin, 2012), pp. 273–330.
- <sup>21</sup>T. Wadsten, R. G. Hazel, S. E. Rasmussen, D. Heinegard, A. T. Balaban, and J. C. Craig, *Acta Chem. Scand.* **23**(7), 2532–2533 (1969).
- <sup>22</sup>R. B. Fair and J. Tsai, *J. Electrochem. Soc.* **124**(7), 1107–1118 (1977).
- <sup>23</sup>D. Shaw, *Phys. Status Solidi B* **72**(1), 11–39 (1975).
- <sup>24</sup>P. M. Fahey, P. B. Griffin, and J. D. Plummer, *Rev. Mod. Phys.* **61**(2), 289–384 (1989).
- <sup>25</sup>J. S. Makris and B. J. Masters, *J. Electrochem. Soc.* **120**(9), 1252 (1973).
- <sup>26</sup>A. Ural, P. B. Griffin, and J. D. Plummer, *J. Appl. Phys.* **85**(9), 6440–6446 (1999).
- <sup>27</sup>S. M. Hu, P. Fahey, and R. W. Dutton, *J. Appl. Phys.* **54**(12), 6912–6922 (1983).
- <sup>28</sup>R. Hull, *Properties of Crystalline Silicon* (The Institution of Electrical Engineers, London, 1999), pp. 885–992.
- <sup>29</sup>F. A. Trumbore, *Bell Syst. Tech. J.* **39**(1), 205–233 (1960).
- <sup>30</sup>E. Kooi, *J. Electrochem. Soc.* **111**(12), 1383 (1964).
- <sup>31</sup>J. Speight, *Lange's Handbook of Chemistry* (McGraw-Hill Education, New York, 2005), p. 151.
- <sup>32</sup>W. Cao, S.-L. Chen, F. Zhang, K. Wu, Y. Yang, Y. A. Chang, R. Schmid-Fetzer, and W. A. Oates, *CALPHAD* **33**(2), 328–342 (2009).
- <sup>33</sup>See <https://computherm.com/products> for information about Pandat Software.
- <sup>34</sup>S. Ohno, M. Hirao, and M. Kido, *Carb. Res.* **108**(2), 163–171 (1982).
- <sup>35</sup>B. S. Krumgalz, *J. Phys. Chem. Ref. Data* **46**(4), 043101 (2017).
- <sup>36</sup>J. Sui, Y. Luo, J. Zhai, F. Fan, L. Zhang, J. Lu, and X. Zhu, *J. Mol. Liq.* **304**(1), 112723 (2020).
- <sup>37</sup>K. C. Russell, *Adv. Colloid Interface Sci.* **13**(3), 205–318 (1980).
- <sup>38</sup>R. Wagner, R. Kampmann, and P. W. Voorhees, *Phase Transformations in Materials* (Wiley-VCH Verlag GmbH, Weinheim, 2001), pp. 314–344.
- <sup>39</sup>T. Y. Tan and W. J. ToyIor, *Semiconductors and Semimetals: Oxygen in Silicon* (Academic Press, New York, 1994), pp. 353–387.
- <sup>40</sup>A. T. Dinsdale, *CALPHAD* **15**(4), 317–425 (1991).
- <sup>41</sup>F. R. N. Nabarro, *Proc. R. Soc. London. Ser. A* **175**(963), 519–538 (1940).
- <sup>42</sup>H. J. McSkimin and P. Andreatch, Jr., *J. Appl. Phys.* **35**(11), 3312–3319 (1964).
- <sup>43</sup>J. J. Hall, *Phys. Rev.* **161**(3), 756–761 (1967).
- <sup>44</sup>M. A. Hopcroft, W. D. Nix, and T. W. Kenny, *J. Microelectromech. Syst.* **19**(2), 229–238 (2010).
- <sup>45</sup>B. Sonderegger and E. Kozechnik, *Metall. Mater. Trans. A* **40**(3), 499–510 (2009).
- <sup>46</sup>B. Sonderegger and E. Kozechnik, *Metall. Mater. Trans. A* **41**(12), 3262–3269 (2010).
- <sup>47</sup>Y. B. Zeldovich, *Acta Physicochim. USSR* **18**(1), 1 (1943).
- <sup>48</sup>J. Svoboda, F. Fischer, P. Fratzl, and E. Kozechnik, *Mater. Sci. Eng., A* **385**(1), 166 (2004).
- <sup>49</sup>T. J. Shqffirr and D. K. Schrodrir, *Semiconductors and Semimetals: Oxygen in Silicon* (Academic Press, New York, 1994), pp. 53–86.
- <sup>50</sup>A. Borghesi, B. Pivac, A. Sassella, and A. Stella, *J. Appl. Phys.* **77**(9), 4169–4244 (1995).
- <sup>51</sup>F. S. Ham, *J. Phys. Chem. Solids* **6**(4), 335–351 (1958).
- <sup>52</sup>S. Hu, *Mater. Sci. Eng. R: Rep.* **13**(3), 105–192 (1994).